Journal of Applied Mechanics and Technical Physics, Vol. 49, No. 3, pp. 354–361, 2008

INVESTIGATION OF STEADY LAMINAR FLOWS WITH AN INITIAL DISTURBANCE

A. M. Lipanov and S. A. Karskanov

UDC 519.6

Results of a parametric study of steady asymmetric flows are analyzed. Three-dimensional unsteady equations of hydromechanics for a compressible medium are solved by a time-dependent method. The range of the characteristic Reynolds number $\mathrm{Re} = 60$–350 *is considered. It is shown that a symmetric flow becomes asymmetric at* $\mathrm{Re} = 90$. *This value can be considered as a threshold value for air. In the examples considered, the upper separation region is always smaller than the lower separation region owing to flow asymmetry in the vicinity of the left boundary of the domain of integration. The dependence of the separation region size on the Reynolds number is found.*

Key words: *equations of hydromechanics, Reynolds number, Mach number, Prandtl number, domain of integration, separation region.*

Steady laminar flows have been well studied both experimentally and theoretically, in contrast to unsteady laminar and turbulent flows [1]. Nevertheless, no detailed parametric investigations were performed, in particular, for compressible media.

A compressible symmetric laminar flow becomes one-dimensional far from the left boundary of the channel (channel entrance) and can be described by the equality

$$\rho U = \text{const},$$

where ρ is a function of the gas velocity U. As a result, a Poiseuille profile is not formed for a compressible laminar flow [2]. If the characteristic Reynolds number Re is greater than a certain value Re_1, then the laminar flow becomes asymmetric [3]. The range of Reynolds numbers $\mathrm{Re} = 60$–350 considered in the paper is typical of various engineering devices (water-supply pipes, channels of gas-dynamic communication in flying vehicles, etc.).

For studying symmetric and asymmetric compressible laminar flows, we consider a channel with a sudden change in the cross-sectional area at the entrance (Fig. 1). The channel is a cavity between two surfaces, which is unbounded in the z direction.

The following system of three-dimensional unsteady differential equations is solved:

$$\frac{\partial \rho}{\partial t} + \frac{\partial \rho U}{\partial x} + \frac{\partial \rho V}{\partial y} + \frac{\partial \rho W}{\partial z} = 0,$$

$$\frac{\partial \rho U}{\partial t} + \frac{\partial}{\partial x}\Big(\frac{p}{k\mathrm{M}^2} + \rho U^2\Big) + \frac{\partial \rho UV}{\partial y} + \frac{\partial \rho UW}{\partial z}$$

$$= \frac{1}{\mathrm{Re}}\Big\{\frac{\partial}{\partial x}\Big[\frac{4}{3}\frac{\partial U}{\partial x} - \frac{2}{3}\Big(\frac{\partial V}{\partial y} + \frac{\partial W}{\partial z}\Big)\Big] + \frac{\partial}{\partial y}\Big(\frac{\partial U}{\partial y} + \frac{\partial V}{\partial x}\Big) + \frac{\partial}{\partial z}\Big(\frac{\partial U}{\partial z} + \frac{\partial W}{\partial x}\Big)\Big\},$$

Institute of Applied Mechanics, Ural Division, Russian Academy of Sciences, Izhevsk 426067; ipm@udman.ru; ser@udman.ru. Translated from Prikladnaya Mekhanika i Tekhnicheskaya Fizika, Vol. 49, No. 3, pp. 11–19, May–June, 2008. Original article submitted December 5, 2006; revision submitted May 31, 2007.

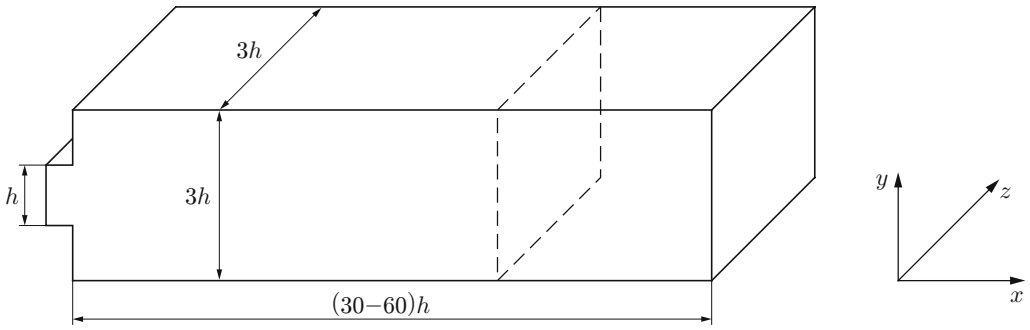

Fig. 1. Domain of integration.

$$
\begin{gathered}
\frac{\partial \rho V}{\partial t}+\frac{\partial \rho V U}{\partial x}+\frac{\partial}{\partial y}\Big(\frac{p}{k\mathrm{M}^2}+\rho V^2\Big)+\frac{\partial \rho V W}{\partial z} \\
=\frac{1}{\mathrm{Re}}\Big\{\frac{\partial}{\partial x}\Big(\frac{\partial U}{\partial y}+\frac{\partial V}{\partial x}\Big)+\frac{\partial}{\partial y}\Big[\frac{4}{3}\,\frac{\partial V}{\partial y}-\frac{2}{3}\Big(\frac{\partial U}{\partial x}+\frac{\partial W}{\partial z}\Big)\Big]+\frac{\partial}{\partial z}\Big(\frac{\partial V}{\partial z}+\frac{\partial W}{\partial y}\Big)\Big\}, \\
\frac{\partial \rho W}{\partial t}+\frac{\partial \rho W U}{\partial x}+\frac{\partial \rho W V}{\partial y}+\frac{\partial}{\partial z}\Big(\frac{p}{k\mathrm{M}^2}+\rho W^2\Big) \\
=\frac{1}{\mathrm{Re}}\Big\{\frac{\partial}{\partial x}\Big(\frac{\partial U}{\partial z}+\frac{\partial W}{\partial x}\Big)+\frac{\partial}{\partial y}\Big(\frac{\partial V}{\partial z}+\frac{\partial W}{\partial y}\Big)+\frac{\partial}{\partial z}\Big[\frac{4}{3}\,\frac{\partial W}{\partial z}-\frac{2}{3}\Big(\frac{\partial U}{\partial x}+\frac{\partial V}{\partial y}\Big)\Big]\Big\}, \\
\frac{\partial \rho E}{\partial t}+\frac{\partial}{\partial x}\Big[\Big(\frac{p}{k\mathrm{M}^2}+\rho E\Big)U\Big]+\frac{\partial}{\partial y}\Big[\Big(\frac{p}{k\mathrm{M}^2}+\rho E\Big)V\Big]+\frac{\partial}{\partial z}\Big[\Big(\frac{p}{k\mathrm{M}^2}+\rho E\Big)W\Big] \\
=\frac{1}{\mathrm{Re}}\Big\{-\frac{2}{3}\,\frac{\partial}{\partial x}\Big[U\Big(\frac{\partial U}{\partial x}+\frac{\partial V}{\partial y}+\frac{\partial W}{\partial z}\Big)\Big]+2\,\frac{\partial}{\partial x}\Big(U\,\frac{\partial U}{\partial x}\Big)+\frac{\partial}{\partial x}\Big[V\Big(\frac{\partial U}{\partial y}+\frac{\partial V}{\partial x}\Big)\Big] \\
+\frac{\partial}{\partial x}\Big[W\Big(\frac{\partial U}{\partial z}+\frac{\partial W}{\partial x}\Big)\Big]+\frac{\partial}{\partial y}\Big[U\Big(\frac{\partial U}{\partial y}+\frac{\partial V}{\partial x}\Big)\Big]+\frac{\partial}{\partial y}\Big[W\Big(\frac{\partial V}{\partial z}+\frac{\partial W}{\partial y}\Big)\Big] \\
-\frac{2}{3}\,\frac{\partial}{\partial y}\Big[V\Big(\frac{\partial U}{\partial x}+\frac{\partial V}{\partial y}+\frac{\partial W}{\partial z}\Big)\Big]+2\,\frac{\partial}{\partial y}\Big(V\frac{\partial V}{\partial y}\Big)+\frac{\partial}{\partial z}\Big[U\Big(\frac{\partial U}{\partial z}+\frac{\partial W}{\partial x}\Big)\Big] \\
+\frac{\partial}{\partial z}\Big[V\Big(\frac{\partial V}{\partial z}+\frac{\partial W}{\partial y}\Big)\Big]-\frac{2}{3}\,\frac{\partial}{\partial z}\Big[W\Big(\frac{\partial U}{\partial x}+\frac{\partial V}{\partial y}+\frac{\partial W}{\partial z}\Big)\Big]+2\frac{\partial}{\partial z}\Big(W\frac{\partial W}{\partial z}\Big)+\frac{1}{(k-1)\mathrm{M}^2\mathrm{Pr}}\Big(\frac{\partial^2 T}{\partial x^2}+\frac{\partial^2 T}{\partial y^2}+\frac{\partial^2 T}{\partial z^2}\Big)\Big\}.
\end{gathered}
\tag{1}
$$

Equations (1) are written in dimensionless variables in an orthogonal Cartesian coordinate system and have a divergent form. As a result, the following parameters are found under the signs of partial derivatives with respect to time: gas density ρ, components of the flow density vector ρU, ρV, and ρW, and total energy of a unit volume ρE. The variables ρ, ρU, ρV, ρW, and ρE are unknown; they are determined by solving Eqs. (1). The remaining gas-dynamic parameters are expressed via these five variables.

To calculate the components U, V, and W of the flow velocity vector, we use the formulas

$$U=\frac{\rho U}{\rho}, \qquad V=\frac{\rho V}{\rho}, \qquad W=\frac{\rho W}{\rho}.$$

The pressure is found from the expression [3]

$$p=k(k-1)\mathrm{M}^2\Big(\rho E-\frac{(\rho U)^2+(\rho V)^2+(\rho W)^2}{2\rho}\Big),$$

and the temperature is calculated with the use of the Clapeyron–Mendeleev equation of state

$$p=\rho RT$$

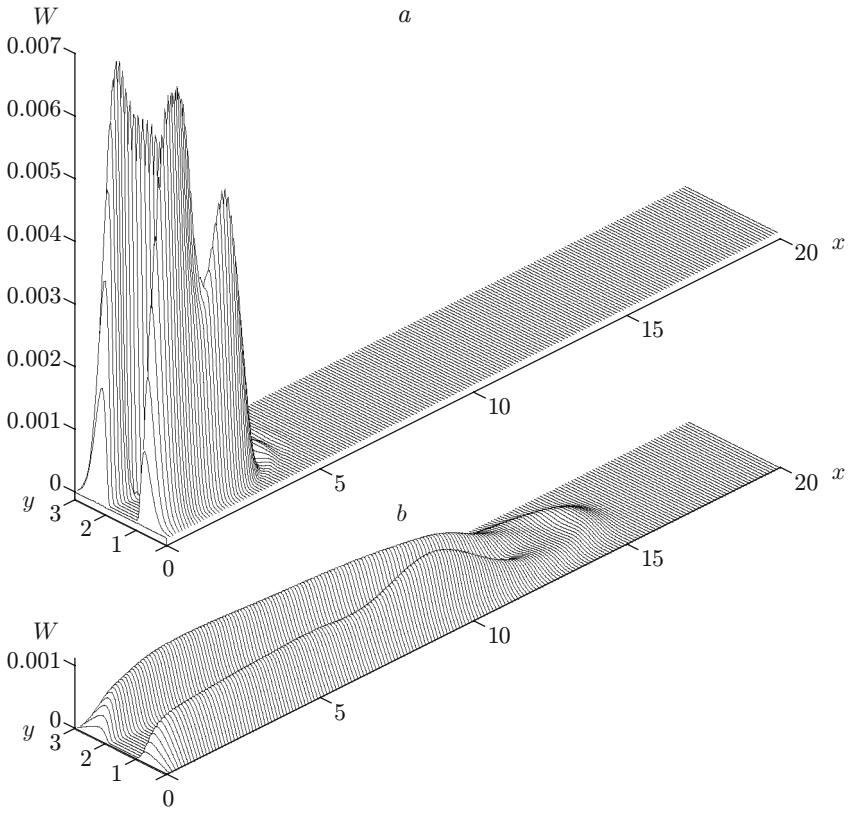

Fig. 2. Evolution of the component W of the flow velocity vector for $\mathrm{Re} = 200$ and $t = 5.6$ (a) and 28 (b).

by the formula

$$T = k(k-1)\mathrm{M}^2\Big(\frac{\rho E}{\rho} - \frac{(\rho U)^2 + (\rho V)^2 + (\rho W)^2}{2\rho^2}\Big)$$

(E is the specific energy of the gas). Equations (1) contain the dimensional complexes

$$\mathrm{Re} = \frac{\rho_* U_* h}{\mu}, \quad \mathrm{Pr} = \frac{C_p \mu}{\lambda}, \quad \mathrm{M} = \frac{U_*}{c_*}, \quad c_* = \Big(\frac{k p_*}{\rho_*}\Big)^{1/2}, \quad k = \frac{C_p}{C_v},$$

where U_* is the maximum value of the longitudinal component of the flow velocity vector at the channel entrance, p_* and ρ_* are the gas pressure and density corresponding to U_*, μ and λ are the viscosity and thermal conductivity, which were assumed to be constant in the present work, and C_p and C_v are the specific heats of the gas at constant pressure and constant volume.

The quantities U_*, p_*, ρ_*, and h were used as scales for the components of the velocity vector, pressure, density, and linear sizes, respectively. The dimensionless time was calculated by the formula

$$t_* = h/U_*.$$

In solving Eqs. (1), we imposed the following initial conditions:

$$U = V = W = 0, \qquad p = p_{\mathrm{in}}, \qquad T = T_{\mathrm{in}}.$$

The boundary conditions for the velocity vector components at the channel entrance were

$$V_0 = W_0 = 0; \tag{2}$$

$$U_0 = \varphi(y, \delta_U) + C_1(P_0 - \langle P\rangle)\varphi(y, \delta_S); \tag{3}$$

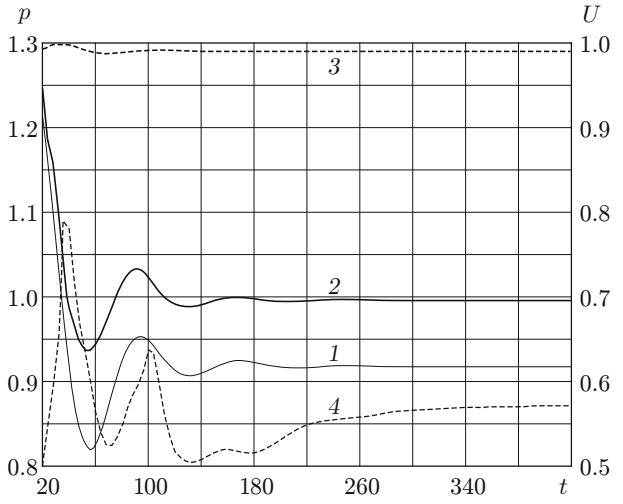

Fig. 3

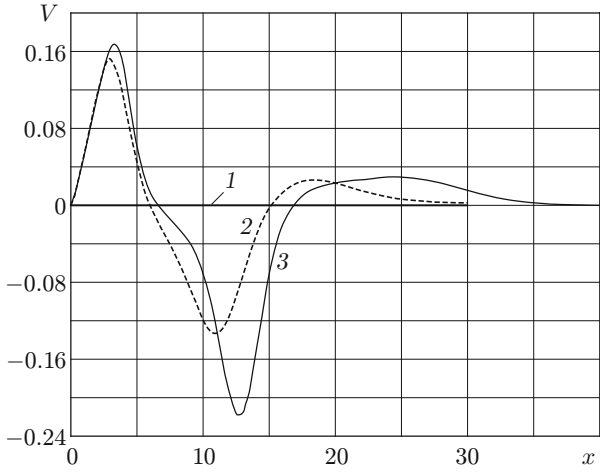

Fig. 4

Fig. 3. Time evolution of flow parameters for Re = 200: curves 1 and 2 show the pressure at the channel entrance (1) and at the point (15, 1.5, 0) (2); curves 3 and 4 show the longitudinal component of velocity at the channel entrance (3) and at the point (15, 1.5, 0) (4).

Fig. 4. Component V of the flow velocity vector along the channel ($Y = 1.5$ and $Z = 0$) for the Reynolds numbers Re = 90 (1), 200 (2), and 350 (3).

$$\varphi(y,\delta_\xi)=\begin{cases}1-(1-y/\delta_\xi)^N, & 0\leqslant y\leqslant\delta_\xi,\\ 1, & \delta_\xi<y\leqslant h-\delta_\xi, \qquad \xi\to(U,S),\\ 1-((y-h+\delta_\xi)/\delta_\xi)^N, & h-\delta_\xi<y\leqslant h,\end{cases}$$

and the entropy function S_0 in the core flow at the channel entrance was subjected to the condition

$$p_0 = S_0\rho_0^k.$$

Here δ_U and δ_S are the thicknesses of the dynamic and thermal boundary layers, N is the order of approximation of the expression used to calculate the partial derivatives of hydrodynamic parameters with respect to the spatial coordinates, the coefficient C_1 is determined by the formula $C_1 = 1/(k\mathrm{M})$ [4], and $\langle P\rangle$ is the mean pressure at the channel entrance.

The difference $P_0 - \langle P\rangle$ averaged over the channel cross section at the channel entrance equals zero, though it differs from zero at any individual value of y. For this reason, condition (3) is unsteady and allows the disturbances reaching the left boundary of the channel to be "removed" outside the domain of integration.

The condition imposed at the channel exit was

$$p = p_a + C_2\sigma(t), \tag{4}$$

where p_a is the dimensionless pressure of the ambient medium, C_2 is a variable quantity determined by the formula [4]

$$C_2 = \frac{k\mathrm{M}}{2H + \mathrm{M}\,\langle m\rangle(t)}; \tag{5}$$

$$\sigma(t) = m(L,t) - \langle m\rangle(t); \tag{6}$$

where

$$\langle m\rangle(t) = \frac{1}{L}\int\limits_S m(x,t)\,dx, \qquad m(x,t) = \iint\limits_{S(x)} \rho U\,dy\,dz, \qquad m(L,t) = \iint\limits_{S(L)} \rho U\,dy\,dz,$$

L is the channel length, H is the half-height of the channel on the right boundary (in the y direction), and $S(x)$ is the cross-sectional area of the channel. The difference $m(L,t) - \langle m\rangle(t)$ in Eq. (6) is sign-variable and allows disturbances to be removed outside the domain of integration through the right boundary of the channel. The remaining parameters (U, V, W, and T) at the exit are determined by extrapolation with a prescribed accuracy from internal points to the boundary along the x axis.

The wetted surfaces were subjected to the no-slip conditions

$$U = V = W = 0,$$

and also the condition of adiabaticity

$$\frac{\partial T}{\partial n} = 0,$$

because we considered flow regimes where the flow temperature was close to the surface temperature.

To select a finite-size volume within an infinitely large domain of integration in the z direction, we regarded one plane of the channel $z = \text{const}$ as a plane of symmetry $z = 0$. After that, we imposed periodicity conditions at a distance $\pm H_z$ from the plane of symmetry $z = 0$:

$$U_+ = U_-, \quad V_+ = V_-, \quad W_+ = W_-, \quad p_+ = p_-, \quad \rho_+ = \rho_-.$$

The distance H_z was assumed to be equal to 1.5. The value of H_z was accepted in [5] and was chosen in [3] for $\mathrm{M} \leqslant 0.6$ and $\mathrm{Re} \leqslant 10^4$.

In addition to the above-mentioned conditions, a three-dimensional disturbance was set at the channel entrance. For this purpose, the velocity vector components V_0 and W_0 at the first 100 steps of integration with respect to time were calculated by the formulas

$$V_0 = W_0 = 0.1U_0. \tag{7}$$

Hence, the flow at the channel entrance during the time interval $t = 0$–0.2 was three-dimensional and directed to the left and upward. After the time $t = 0.2$ (100 steps of integration with respect to time), conditions (7) were replaced by conditions (2). The channel length was $L = 30$ for $\mathrm{Re} \leqslant 200$ and $L = 60$ for $\mathrm{Re} > 200$.

The first and second partial derivatives with respect to the spatial variables were calculated by the method developed in [6] with allowance for the recommendations proposed in [3]. Integration with respect to time was performed by an explicit-implicit scheme with the second order of accuracy.

The evolution of the three-dimensional disturbance inserted into the flow can be traced on the basis of the space and time variations of the velocity vector component W (Fig. 2). In this case, we have $\mathrm{Re} = 200$ when the flow is asymmetric.

As in the case of a symmetric flow, there are two "humps" beginning in the separation regions. In contrast to a symmetric flow, however, the maximums of these humps do not coincide. The distribution of $W(x)$ is nonmonotonic. The maximum of the dependence $W(x)$ is located closer to the channel entrance.

Figure 2a shows the dependence $W(x, y)$ for $z = 0$ for the time $t = 5.6$ after 2800 steps of integration with respect to time, which corresponds to the stage of the process evolution when the equality $\partial W/\partial x\|_{x=0} = 0$ starts being satisfied. The disturbance is shifted inward the channel to a distance $x \approx 5$. The component W decreases with time. At $t = 28$, the value of this component is already smaller than that at $t = 5.6$ by an order of magnitude, and its influence on hydrodynamic parameters may be neglected. By this time, the disturbance propagates to a distance $x > 15$, the total length of the channel being $L = 30$. Thus, the disturbance inserted into the channel decays before it reaches the right boundary. Under these conditions, the hydrodynamic parameters behave in an unsteady manner. Moreover, the channel is filled by a two-dimensional unsteady flow.

At the same value of the Reynolds number $\mathrm{Re} = 200$, the pressure p and the longitudinal component U of the flow velocity vector on the left boundary change with time until $t = 280$ (Fig. 3).

Further downstream, some parameters remain unsteady during a longer time. Thus, for $x = 15$, the longitudinal component U remains time-dependent almost twice longer (curve 4 in Fig. 3), though the pressure reaches the steady state almost at the same time as for $x = 0$ (curve 2 in Fig. 3).

If the characteristic Reynolds number is greater than a certain value, the two-dimensional steady-state flow becomes asymmetric. Figure 4 shows the behavior of the vertical component of the flow velocity vector on the channel axis ($Y = 1.5$, $Z = 0$). The asymmetry is essential near the left boundary. The flow becomes deflected from

TABLE 1

Maximum Friction Stresses and Gradients
of the Vertical Component of the Flow Velocity Vector on the Channel Walls

Re	$(\tau\|_{y=0})_{\max} \cdot 10^5$	$(\tau\|_{y=3})_{\max} \cdot 10^5$	$(\partial V/\partial y\|_{y=0})_{\max}$	$(\partial V/\partial y\|_{y=3})_{\max}$
150	1.176	2.080	0.011	0.020
200	1.722	3.274	0.019	0.035
300	2.966	4.216	0.046	0.064
350	3.380	4.570	0.061	0.078

TABLE 2

Maximums and Minimums of the Vertical Component of the Flow Velocity Vector
on the Axis of Symmetry of the Channel

Re	$V_{\max}$	$\|V_{\min}\|$	Re	$V_{\max}$	$\|V_{\min}\|$
90	0.005	0.003	300	0.168	0.200
120	0.074	0.055	350	0.171	0.218
150	0.122	0.090	400	0.173	0.233
200	0.151	0.134			

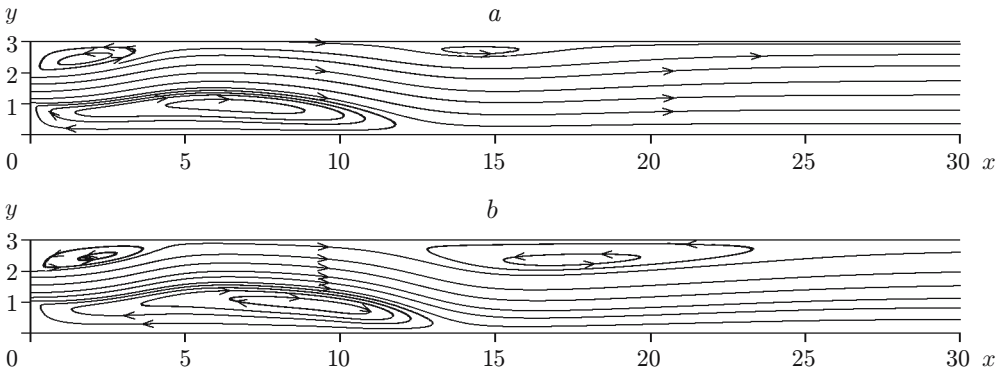

Fig. 5. Streamlines of the steady-state flow for Re = 200 (a) and 300 (b).

the original direction, first upward and then downward. After that, the motion tends to acquire a one-dimensional form and becomes one-dimensional at a distance $x = 38$ for Re = 350. For Re = 200, the one-dimensional flow is observed for $x \geqslant 30$.

As the Reynolds number increases, the maximum friction stresses ($\tau = \mu(\partial U/\partial y)|_{y=0,\,3}$) on the lower and upper walls of the channel also increase (Table 1). The maximum gradients of the vertical component V of the flow velocity vector on the wetted surface also increase in magnitude; they are observed in the vicinity of the point of flow reattachment.

The maximums and minimums (absolute values) of the vertical component of the flow velocity vector on the channel centerline versus Re are listed in Table 2; the threshold value of the Reynolds number is seen to be $\mathrm{Re}_1 = 90$. For $\mathrm{Re} < \mathrm{Re}_1$, the flow is symmetric, and for $\mathrm{Re} > \mathrm{Re}_1$ the absolute values of the vertical component V drastically increase.

Figure 5a shows the streamlines of the flow for Re = 200. Because of flow asymmetry in the vicinity of the left boundary, the upper separation region is substantially smaller than the lower one. Turning around the lower separation region, the flow is deflected downward, and another upper separation region is formed in the interval $13 \leqslant x \leqslant 17$.

An increase in the Reynolds number exerts a noticeable effect on the size of the third separation region. This region is absent for Re = 150, its size for Re = 200 is indicated above, and its size for Re = 300 (Fig. 5b) is almost the same as that of the second separation region.

TABLE 3

Behavior of the Longitudinal and Vertical Components of the Flow Velocity Vector on the Channel Centerline for $\mathrm{Re} = 200$

x	U	V	x	U	V
0	0.990	0	15	0.573	−0.003
3	0.906	0.015	18	0.564	0.026
6	0.510	−0.003	24	0.540	0.008
11	0.725	−0.134	30	0.513	0.001

TABLE 4

Maximum Pressure, Pressure at the Channel Entrance, and Pressure at the Channel Exit

Re	L	p_m	p_0	p_L	x_m
150	30	1.017	0.926	1.002	16.37
200	30	1.003	0.917	1.001	22.50
300	60	1.019	0.937	1.004	33.75
350	60	1.014	0.933	1.004	40.00

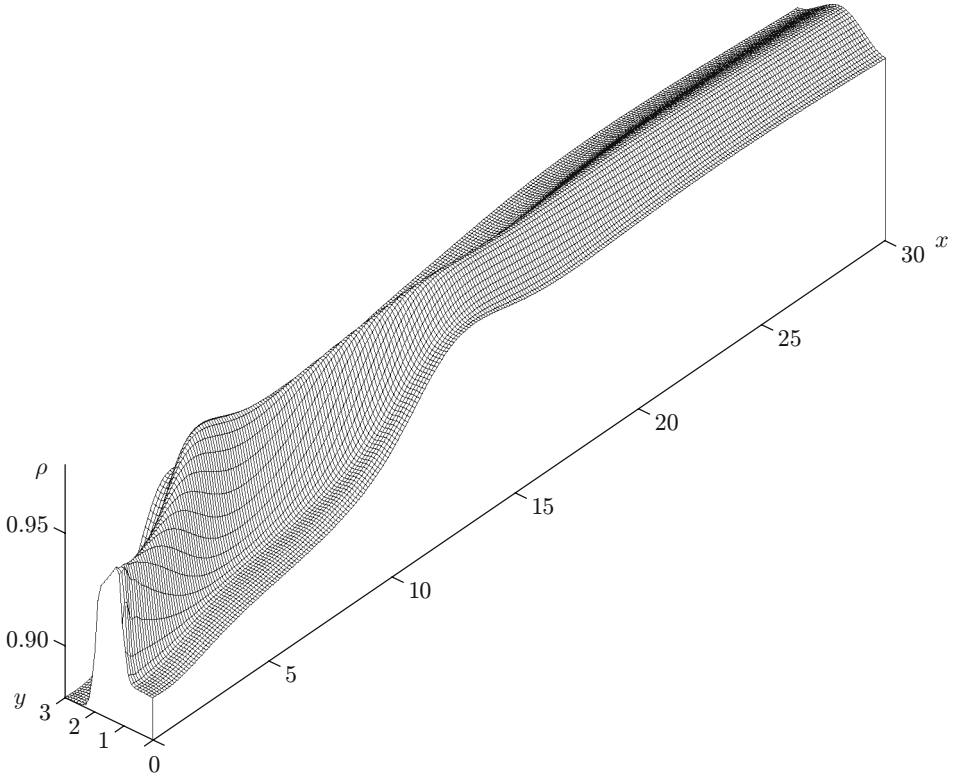

Fig. 6. Density field for $\mathrm{Re} = 200$.

For $\mathrm{Re} = 200$, the steady-state values of the longitudinal and vertical components of the velocity vector (Table 3) vary significantly for $x < 30$, and the flow can be assumed to be one-dimensional only for $x > 30$.

Depending on the x coordinate, the dimensionless pressure p near the left boundary increases and reaches a maximum value p_m at the point x_m; then the pressure decreases to $p_L \approx 1$ on the right boundary of the channel. The value of p_m increases with increasing channel length and decreases with increasing Reynolds number. Some results on the calculated variations of pressure are given in Table 4.

Figure 6 shows the density field in the plane (x, y). Its configuration corresponds to a one-dimensional flow only for $x > 25$.

This work was supported by the Russian Foundation for Basic Research (Grant No. 07-08-96044-r_ural_a) and by the Grant for Young Scientists and Ph.D. Students of the Ural Division of the Russian Academy of Sciences.

REFERENCES

1. N. E. Kochin, I. A. Kibel, and N. V. Rose, *Theoretical Hydromechanics* [in Russian], Fizmatgiz, Moscow (1963).
2. A. M. Lipanov and S. A. Karskanov, "Stabilization and evolution of parameters of a symmetric laminar flow in a plane channel with sudden expansion," *J. Appl. Mech. Tech. Phys.*, **48**, No. 1, 27–33 (2007).
3. A. M. Lipanov, Yu. F. Kisarov, and I. G. Klyuchnikov, *Numerical Experiment in Classical Hydromechanics of Turbulent Flows* [in Russian], Izd. Ural. Otd. Ross. Akad. Nauk, Ekaterinburg (2001).
4. A. T. Fedorchenko, "Problem of removing vortices through a permeable boundary of the calculated domain of an unsteady subsonic flow," *Zh. Vychisl. Mat. Mat. Fiz.*, **26**, No. 1, 114–129 (1986).
5. B. L. Rozhdestvenskii and I. N. Simakin, "Modeling of turbulent flows in a plane channel," *Zh. Vychisl. Mat. Mat. Fiz.*, **25**, No. 1, 96–121 (1985).
6. S. T. Zalesak, "A physical interpretation of the Richtmyer two-step Lax–Wendroff scheme, and its generalization to higher spatial order," in: *Advances in Computer Methods for Partial Differential Equations*, Proc. of the 5th IMACS Int. Symp. on Computer Methods for Partial Differential Equations (Bethlehem, June 19–21, 1984), Rutgers Univ. Press, New Brunswick (1984), pp. 491–496.